Rods of Neutron Scattering Intensity in $Yb_2Ti_2O_7$: Compelling Evidence for Significant Anisotropic Exchange in a Magnetic Pyrochlore Oxide

Jordan D. Thompson,[1] Paul A. McClarty,[1] Henrik M. Rønnow,[2] Louis P. Regnault,[3] Andreas Sorge,[4,5] and Michel J. P. Gingras[1,5,6]

[1]*Department of Physics and Astronomy, University of Waterloo, Waterloo, ON, Canada, N2L 3G1*
[2]*Laboratory for Quantum Magnetism, École Polytechnique Fédérale de Lausanne (EPFL), CH-1015 Lausanne, Switzerland*
[3]*CEA-Grenoble, INAC-SPSMS-MDN, 17 rue des Marthyrs, 38054 Grenoble, cedex 9, France*
[4]*Network Dynamics Group, MPI for Dynamics and Self-Organization, Bunsenstr. 10, 37073 Göttingen, Germany*
[5]*Department of Physics and Astronomy, University of Canterbury, Private Bag 4800, Christchurch, New Zealand*
[6]*Canadian Institute for Advanced Research, 180 Dundas Street West, Toronto, Ontario M5G 1Z8, Canada*

(Received 19 September 2010; published 6 May 2011)

Paramagnetic correlations in the magnetic material $Yb_2Ti_2O_7$ have been investigated via neutron scattering, revealing a [111] rod of scattering intensity. Assuming interactions between the Yb^{3+} ions composed of all symmetry-allowed nearest neighbor exchange interactions and long-range dipolar interactions, we construct a model Hamiltonian that allows for an excellent description of the neutron scattering data. Our results provide compelling evidence for significant anisotropic exchange interactions in an insulating magnetic pyrochlore oxide. We also compute the real space correlations leading to the [111] rod of scattering.

DOI: 10.1103/PhysRevLett.106.187202 PACS numbers: 75.10.Hk, 05.50.+q, 75.10.Dg, 75.25.−j

In geometrically frustrated magnetic materials there exists no configuration of magnetic moments that simultaneously satisfies all the pairwise magnetic interactions. Experimental and theoretical research over the past 20 years has shown that frustrated magnetic systems are prone to exhibit novel and intriguing collective thermodynamic phenomena [1].

Among frustrated three dimensional systems, the $A_2B_2O_7$ pyrochlores have attracted much attention [2]. In these compounds, A is a trivalent rare earth ion (Ho, Dy, Tb, Gd, Yb) or yttrium (Y) and B is a tetravalent transition metal ion (Ti, Sn, Mo, Mn). Both A and B reside on two distinct lattices of corner-sharing tetrahedra. Theory predicts that classical [3] and quantum [4] Heisenberg spins on a pyrochlore lattice interacting via an isotropic antiferromagnetic nearest neighbor exchange Hamiltonian, H_H, fail to develop conventional LRO down to zero temperature. In real pyrochlore compounds, however, there generally exists some combination of other perturbing magnetic interactions (e.g., single-ion anisotropy, dipolar interactions, etc.) beyond H_H. Since H_H alone does not produce LRO, the low-temperature magnetic correlations of these materials are strongly influenced by the competition between material-specific perturbations. This is the origin of the richness of phenomena observed in the $A_2B_2O_7$ pyrochlores [2] including spin liquid [5], spin glass [6], spin ice [7], and LRO with persistent low-temperature spin dynamics [8,9]. In this article, we consider the $Yb_2Ti_2O_7$ pyrochlore which does not apparently exhibit any of the aforementioned phenomena and has some unique and unusual features of its own which have heretofore remained unexplained.

$Yb_2Ti_2O_7$ has a ferromagnetic character with a Curie-Weiss temperature, $\theta_{CW} = +0.65 \pm 0.15$ K [10]. The $Yb^{3+} \sim 3\ \mu_B$ magnetic moments predominantly lie perpendicular to the local [111] cubic unit cell diagonals, making this system the only known local [111] XY pyrochlore with a ferromagnetic θ_{CW} [2]. Magnetic specific heat (C_m) measurements reveal a sharp first order transition at $T_c \approx 240$ mK [11], suggesting the onset of LRO. While a single crystal elastic neutron scattering (NS) study suggested ferromagnetic order below T_c [12], a subsequent polarized NS study [13] did not confirm such ordering. Furthermore, powder NS shows no LRO down to 110 mK [14] and very recent NS on a single crystal sample has not found any sign of LRO in a broad region of the (hkk) scattering plane at 30 mK [15]. The $T_c \approx 240$ mK transition seen in C_m has therefore so far not been matched with the observation of conventional (dipolar magnetic) LRO. In addition, Mössbauer spectroscopy and muon spin relaxation (μSR) measurements find a rapid decrease of the Yb^{3+} magnetic moments fluctuation rate, ν, upon approaching T_c from above, with μSR revealing a temperature-independent ν (i.e., persistent spin dynamics) from T_c down to 40 mK, the lowest temperature considered [14]. Considering all these results together, one may ask whether the 240 mK transition in $Yb_2Ti_2O_7$ may be another rare example of hidden (nondipolar) order [16]. Another intriguing possibility [14] is that the 240 mK first order transition takes place between a ''spin gas'' (paramagnetic) state and a spin liquid without any symmetry breaking.

A very interesting feature of the magnetic correlations in $Yb_2Ti_2O_7$ found at temperatures $T_c < T \lesssim 2$ K are rods of NS intensity along the [111] directions [9,15]. At first sight,

the presence of such rods signals an anisotropy in the magnetic correlations that may originate from a structural transition at $T \gtrsim 2$ K or from intrinsically stronger correlations within the kagome planes perpendicular to the four [111] directions forming the undistorted pyrochlore structure as compared to correlations perpendicular to the kagome planes [15]—hence making a "spin liquid crystal" of sorts.

Here, we report results from diffuse NS measurements on $Yb_2Ti_2O_7$ in a temperature range above $\theta_{CW} > T_c$. By numerically annealing a set of exchange couplings to maximize the agreement between experimental results and NS computed within a random phase approximation (RPA), we determine a spin Hamiltonian, H, that captures the main features of the observed paramagnetic NS pattern and reveals that significant spin exchange anisotropy exists in this insulating pyrochlore oxide material. There have been recent claims of evidence for anisotropic exchange at play in $Yb_2Ti_2O_7$ [17,18] and other $A_2B_2O_7$ pyrochlores [17,19]. However, because of the limitations imposed by the physical quantity considered (local susceptibility, χ_{local}), and the models used in these works, the specific nature and symmetry of the putative microscopic exchange has, until this work, remained hidden [20]. Owing to the highly structured spin correction function in $Yb_2Ti_2O_7$, we obtain compelling evidence for anisotropic exchange. From the reciprocal space structure factor, we compute the spin-spin correlations along different crystallographic directions. While these correlations are anisotropic, the correlation lengths themselves do not distinguish between correlations parallel and perpendicular to the kagome planes.

The NS cross section was measured on the D23 diffractometer at the Institut Laue Langevin, France. A single crystal rod was aligned with $[h00]$ and $[0kk]$ in the scattering plane, hence providing access to all principal symmetry directions of the cubic crystal structure. With incident neutron energy of 14.7 meV, significantly larger than any characteristic energy scale in the system, and counting all final energies, the measured intensity is proportional to the spatial Fourier transform of the instantaneous correlation function $S(\mathbf{q}) = \int S(\mathbf{q}, \omega) d\omega$.

Figures 1(a) and 1(b) show experimental NS data for $Yb_2Ti_2O_7$ at $T = 9.1$ K and $T = 1.4$ K in the (hkk) plane. Sharp intense Bragg peaks at integer reciprocal lattice positions were removed from the data to expose significant structure in the diffuse magnetic scattering. Figure 1(a) shows the NS map at $T = 9.1$ K. The magnetic correlations weaken with increasing temperature. Indeed, most of the features present at $T = 1.4$ K [Fig. 1(b)] are absent at 9.1 K, with only a weakened rod of scattering along [111] and a feature in the upper right corner at 3.5, 2.25, 2.25 remaining. Figure 1(b) shows the NS map at $T = 1.4$ K, where the most interesting feature is the aforementioned rod of scattering along the [111] direction [9,15]. Figure 1(b) exhibits other features of interest such as a weaker rod of scattering going from 400 to 222 and intensity near the point 022. The intensity of the feature

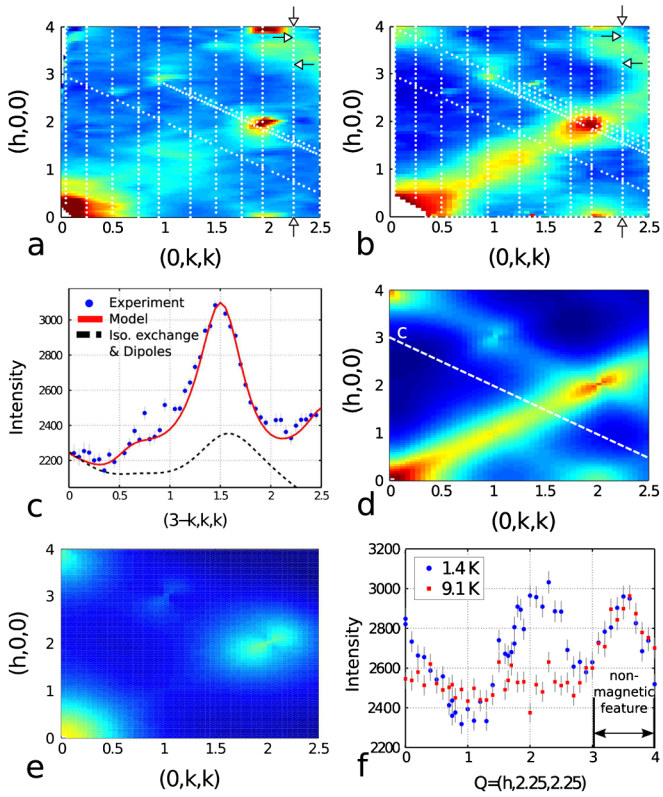

FIG. 1 (color online). Neutron scattering (NS) maps in the (h, k, k) plane. (a) and (b) show experimental data at 9.1 and 1.4 K, respectively. In (b), a rod of scattering intensity along [111] is clearly seen, while in (a) the rod is not strong. (c) shows a comparison between experimental data and the computed NS intensity at 1.4 K along $[3 - k, k, k]$ for both isotropic exchange and the full model. (d) shows computed NS using the Hamiltonian H (see text), at $T = 1.4$ K. (e) shows the calculated NS using H with only isotropic exchange determined from fitting θ_{CW} and long-range dipolar interactions at $T = 1.4$ K. (f) shows experimental neutron scattering at 1.4 and 9.1 K along the line $[h, 2.25, 2.25]$ showing that the feature between $h = 3$ and $h = 4$ does not change in intensity with temperature. The white arrows in (a) and (b) indicate the range $h \in [3, 4]$ in $[h, 2.25, 2.25]$ in (f).

centered on 3.5, 2.25, 2.25 does not change with temperature [Fig. 1(f)] indicating that it is not magnetic in origin and can therefore be omitted from further consideration.

To explain the NS pattern, we propose a Hamiltonian, $H = H_{cf} + H_{int}$, that includes a crystal field (CF) part, H_{cf}, and spin-spin interactions, $H_{int} = H_{dip} + H_{ex}$. The form of H_{cf} is fixed by the symmetry of the Yb^{3+} environment. The two sets of CF parameters that we use have been determined in Refs. [14,17]. The magnetic Yb^{3+} ion has electronic configuration $^2F_{7/2}$, hence $J = 7/2$ and Landé factor $g_J = 8/7$. The nearest neighbor distance between Yb^{3+} ions is $r_{nn} = (a/4)\sqrt{2}$, where $a = 10.026$ Å is the size of the conventional cubit unit cell [13]. This fixes the strength of the coupling $D = \frac{\mu_0 (g_J \mu_B)^2}{4\pi (r_{nn})^3} \approx 0.01848$ K of the long-range magnetostatic dipolar interaction, $H_{dip} = \frac{1}{2} \sum_{(i,a;j,b)} \frac{D(r_{nn})^3}{|\mathbf{R}_{ij}^{ab}|^3} (\mathbf{J}_i^a \cdot \mathbf{J}_j^b - 3(\mathbf{J}_i^a \cdot \hat{\mathbf{R}}_{ij}^{ab})(\mathbf{J}_j^b \cdot \hat{\mathbf{R}}_{ij}^{ab}))$.

We also consider $H_{\rm ex}$ which contains all nearest neighbor exchange interactions, $\mathcal{J}_e$, that respect lattice symmetries. There are four such nearest neighbor interactions [21]: $H_{\rm Ising} = -\mathcal{J}_{\rm Ising}\sum_{\langle i,a;j,b\rangle}(\mathbf{J}_i^a \cdot \hat{\mathbf{z}}^a)(\mathbf{J}_j^b \cdot \hat{\mathbf{z}}^b)$, which couples the local [111] $\hat{z}$ components of $\mathbf{J}$, $H_{\rm iso} = -\mathcal{J}_{\rm iso}\sum_{\langle i,a;j,b\rangle}\mathbf{J}_i^a \cdot \mathbf{J}_j^b$, the standard isotropic exchange, $H_{\rm pd} = -\mathcal{J}_{\rm pd}\sum_{\langle i,a;j,b\rangle}(\mathbf{J}_i^a \cdot \mathbf{J}_j^b - 3(\mathbf{J}_i^a \cdot \hat{\mathbf{R}}_{ij}^{ab})(\mathbf{J}_j^b \cdot \hat{\mathbf{R}}_{ij}^{ab}))$, a pseudodipolar interaction of exchange origin and not part of $H_{\rm dip}$ and, finally, $H_{\rm DM} = -\mathcal{J}_{\rm DM}\sum_{\langle i,a;j,b\rangle}\mathbf{\Omega}_{\rm DM}^{a,b} \cdot (\mathbf{J}_i^a \times \mathbf{J}_j^b)$, the Dzyaloshinskii-Moriya (DM) interaction [22]. In all of these terms, $\mathbf{J}_i^a$ denotes the angular momentum of the Yb^{3+} located at lattice $\mathbf{R}_i^a$ (FCC lattice site i, and tetrahedral sublattice site a) [23] and $\hat{\mathbf{R}}_{ij}^{ab}$ is a unit vector directed along $\mathbf{R}_j^b - \mathbf{R}_i^a$. The relationship between $H_{\rm int}$ and a corresponding effective spin-1/2 model is discussed in the supplemental material [24].

We use H to compute the diffuse NS pattern within the RPA [25,26] (see Ref. [24] for justification of the usage of RPA for the present problem). We first compute the single-ion susceptibility, $\chi^{(0)}$, from $H_{\rm cf}$:

$$\chi_a^{(0),\alpha\beta}(\omega) = \sum_{\mu,\nu}^{E_\mu \neq E_\nu} \frac{M_{\nu\mu,a}^{\alpha} M_{\mu\nu,a}^{\beta}}{E_\mu - E_\nu - \hbar(\omega + i0^+)}(n_\nu - n_\mu) + \frac{\delta(\omega)}{k_B T}\sum_{\mu,\nu}^{E_\mu = E_\nu} M_{\nu\mu,a}^{\alpha} M_{\mu\nu,a}^{\beta} n_\nu, \quad (1)$$

where n_ν is the thermal occupation fraction for CF state ν. $M_{\nu\mu,a}^{\alpha} = \sum_{\bar{\alpha}}\langle\nu|J^{\bar{\alpha}}|\mu\rangle u_{\bar{\alpha},a}^{\alpha}$, where $u_{\bar{\alpha},a}^{\alpha}$ is the rotation matrix from the local ($\bar{\alpha}$) frame defined on sublattice a to the global (α) frame. The operator $\mathbf{J}^{\bar{\alpha}}$ acts on the CF states defined in the local $\bar{\alpha}$ quantization frame. The CF wave functions $|\nu\rangle$, at sublattice site a, are obtained by diagonalizing $H_{\rm cf}$ [14,17]. The interacting RPA susceptibility, $\chi(\mathbf{q},\omega)$ [26], is then $\chi_{ab}^{\alpha\beta}(\mathbf{q},\omega) + \sum_{\gamma,\delta,c}\chi_a^{0,\alpha\gamma}(\omega)\mathcal{J}_{ac}^{\gamma\delta}(\mathbf{q})\chi_{cb}^{\delta\beta}(\mathbf{q},\omega) = \delta_{ab}\chi_a^{0,\alpha\beta}(\omega)$, where $\mathcal{J}(\mathbf{q})$ is the Fourier transformation of the interaction matrix $\mathcal{J}(i,j)$ for Hamiltonian $H_{\rm int} = -(1/2)\sum_{i,j;a,b;\alpha,\beta}J_{i,a}^{\alpha}\mathcal{J}_{ab}^{\alpha\beta}(i,j)J_{j,b}^{\beta}$. The infinite lattice sum of the dipolar interaction is computed using Ewald summation [23]. We solve for $\chi_{ab}^{\alpha\beta}(\mathbf{q},\omega)$ numerically. Finally, the NS function, $S(\mathbf{q},\omega)$ [25,26], is given by

$$S(\mathbf{q},\omega) \propto \frac{|f(\mathbf{Q})|^2}{k_B T}\sum_{\alpha,\beta}\sum_{a,b}(\delta_{\alpha\beta} - \hat{Q}_\alpha\hat{Q}_\beta) \times \exp(-i(\mathbf{r}^a - \mathbf{r}^b)\cdot\mathbf{G})\mathrm{Re}(\chi_{ab}^{\alpha\beta}(\mathbf{q},\omega)) \quad (2)$$

where $f(\mathbf{Q})$ is the magnetic form factor for the Yb^{3+} ion [27]. $\mathbf{Q} = \mathbf{q} + \mathbf{G}$ is the scattering wave vector where $\mathbf{q}$ is a wave vector inside the first Brillouin zone, and $\mathbf{G}$ is an FCC reciprocal lattice vector. $\mathbf{r}^a$ and $\mathbf{r}^b$ are basis vectors for the tetrahedral sublattice [23].

The fit to the experimental data was performed by computing the RPA scattering intensity along the measured lines in $\mathbf{Q}$ space [white dashed lines in Fig. 1(b)]. The computed intensities were rescaled to the experimental count rate using the relation $S'(\mathbf{q}) = c_0 S(\mathbf{q}) + c_1 + c_2|\mathbf{Q}|$ [28], where the parameters c_0, c_1, and c_2 are the same for all $\mathbf{Q}$ points. There are therefore seven adjustable parameters in total with the four exchange couplings, $\mathcal{J}_e$ and the three c_n fitting parameters. The variance between the measured and calculated neutron data, with a contribution to the variance from fitting $\theta_{\rm CW}$ as well, was minimized using a simulated annealing algorithm [29]. As a first step, for simplicity and computational speed, we make a static approximation [30] to $S(\mathbf{q},\omega)$. Within the moderate constraints (see supplemental material [24]) of the procedure followed, the present calculation is suitable to reach the main conclusion of this work: that significant anisotropic exchange couplings $\mathcal{J}_e$ are necessary to account for the structure of the NS pattern of $Yb_2Ti_2O_7$.

Figure 1(d) shows the RPA NS pattern in the (hkk) plane at 1.4 K obtained from simulated annealing fits to the experimental neutron scattering map of Fig. 1(b). The model data in Fig. 1(d) are obtained using $H_{\rm cf}$ from Ref. [17] and from a $H_{\rm ex}$ with $\mathcal{J}_{\rm Ising} = 0.76$ K, $\mathcal{J}_{\rm iso} = 0.18$ K, $\mathcal{J}_{\rm pd} = -0.26$ K, and $\mathcal{J}_{\rm DM} = -0.25$ K. The calculated intensity matches the experimental data [Fig. 1(b)] well, providing strong evidence that our model $H_{\rm ex}$ contains the correct interactions for $Yb_2Ti_2O_7$. A cut along $[3-k,k,k]$ [Fig. 1(c)] emphasizes the quantitative agreement between the computed and experimental NS intensities. A similar quality of fit was obtained for other line scans [dashed lines in Fig. 1(b)], as shown in the supplemental material [24]. We carried out the fitting procedure using CF parameters for $H_{\rm cf}$ taken from Refs. [14,17] finding that the exchange couplings do not change significantly. Figure 1(e) and the dashed (black) line in Fig. 1(c) show the NS intensity calculated for a model $H_{\rm int}$ with only long-range dipolar and isotropic exchange interactions ($\mathcal{J}_{\rm Ising} = \mathcal{J}_{\rm pd} = \mathcal{J}_{\rm DM} = 0$) with $\mathcal{J}_{\rm iso} = 0.06$ K, determined by fitting $\theta_{\rm CW}$, and refitted c_n's. Clearly this model and the resulting NS pattern do not describe the experimental data [Fig. 1(b)] well at all. Similarly, a Hamiltonian with isotropic-only exchange does not describe the local susceptibility, $\chi_{\rm local}$, well [17–20]. On the other hand, the present anisotropic Hamiltonian describes $\chi_{\rm local}$ with no adjustable parameters [20].

To rationalize the direct space origin of rods of NS intensity, we computed the spin-spin correlation function from the reciprocal space RPA susceptibility $\langle J_a^\alpha(\mathbf{r})J_b^\beta(\mathbf{0})\rangle = k_B T\int\chi_{ab}^{\alpha\beta}(\mathbf{q})\exp(\mathbf{q}\cdot\mathbf{r})d\mathbf{q}$ where $\mathbf{r} = \mathbf{R}_j^b - \mathbf{R}_i^a$. The integral was performed numerically over the first Brillouin zone. We considered the isotropic real space correlations (by summing over all directions α in spin space) $S(\mathbf{r}) \equiv \sum_\alpha\langle J_a^\alpha(\mathbf{r})J_b^\alpha(\mathbf{0})\rangle$, and also $S_\perp(\mathbf{r}) \equiv k_B T\int[\delta_{\alpha\beta} - \hat{q}_\alpha\hat{q}_\beta]\chi_{ab}^{\alpha\beta}(\mathbf{q})\exp(\mathbf{q}\cdot\mathbf{r})d\mathbf{q}$ whose Fourier transform is measured in the NS. Figure 2 shows $S(\mathbf{r})$ and $S_\perp(\mathbf{r})$ for $\mathbf{r}$ taken along the [111] direction, and $[0\bar{1}1]$, $[1\bar{2}1]$ perpendicular to [111]. $S(\mathbf{r})$ and $S_\perp(\mathbf{r})$ are

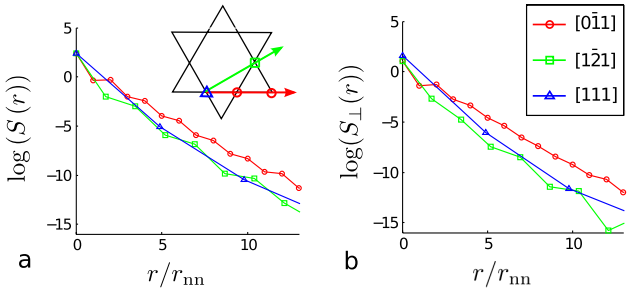

FIG. 2 (color online). Real space spin-spin correlation functions (a) $S(\mathbf{r})$ and (b) $S_\perp(\mathbf{r})$ (see text) computed at $T = 1.4$ K using the anisotropic exchange model and plotted along various crystallographic directions.

similar, so we discuss both together. The correlation lengths for these three directions were extracted, assuming exponential decay, and found not to differ greatly within our margin of error. However, the $[0\bar{1}1]$ correlations are larger than those of the other two directions indicating some degree of spontaneous decoupling of the kagome planes albeit perhaps with a quasi-isotropic correlation length. Since the $[0\bar{1}1]$ directions lie within two kagome planes and the $[1\bar{2}1]$ directions lie in only one, truly two-dimensional correlations may have been be expected to lead to the splitting $S(\mathbf{r})_{[0\bar{1}1]} > S(\mathbf{r})_{[1\bar{2}1]} > S(\mathbf{r})_{[111]}$. This is not borne out by our results—the similarity of $S(\mathbf{r})$ for the $[1\bar{2}1]$ and [111] directions indicates that the correlations are strongest along spin chains. Whereas the NS intensity in the (hhk) plane, considered on its own, suggests that the correlations are quasi two-dimensional [15], with a weak decoupling of the kagome planes, the real space correlations within our model do not support this simple picture.

From the determined H_{ex}, RPA predicts a second order phase transition to a ferromagnetic phase (ordering wave vector $\mathbf{q} = 0$) at a critical temperature $T_c^{\mathrm{RPA}} \approx 1.2$ K. We expect thermal and quantum fluctuations to renormalize the values of the anisotropic exchange $\mathcal{J}_e$ determined above.

In summary, we have presented diffuse neutron scattering (NS) maps of $Yb_2Ti_2O_7$ in its paramagnetic regime, finding rods of scattering in the $\langle 111 \rangle$ directions. By fitting this data to NS computed from a candidate microscopic Hamiltonian, we found a set of couplings that reproduce the main features of this NS pattern. The Hamiltonian includes, as an essential component, sizeable anisotropic exchange interactions. This suggests that anisotropic exchange might be important in other $A_2B_2O_7$ rare earth magnets [17,19]. We find that the rods of scattering occur without any symmetry breaking from, for example, a structural phase transition. We anticipate that our results will allow for a greater understanding of the nature of the phase transition at 240 mK and of the low-temperature phase of $Yb_2Ti_2O_7$.

We thank M. Enjalran and Y.-J. Kao for useful discussions and contributions at the earliest stage of this project. We acknowledge useful discussions with B. Gaulin, K. Ross, and J. Ruff. This work was funded by the NSERC of Canada and the CRC Program (M.G., Tier 1).

[1] H. T. Diep, *Frustrated Spin Systems* (World Scientific, Hackensack, 2004).
[2] J. S. Gardner, M. J. P. Gingras, and J. E. Greedan, Rev. Mod. Phys. **82**, 53 (2010).
[3] R. Moessner and J. T. Chalker, Phys. Rev. Lett. **80**, 2929 (1998).
[4] B. Canals and C. Lacroix, Phys. Rev. Lett. **80**, 2933 (1998).
[5] J. S. Gardner *et al.*, Phys. Rev. Lett. **82**, 1012 (1999).
[6] M. J. P. Gingras *et al.*, Phys. Rev. Lett. **78**, 947 (1997).
[7] S. T. Bramwell and M. J. P. Gingras, Science **294**, 1495 (2001).
[8] Y. Chapuis *et al.*, Physica (Amsterdam) **404B**, 686 (2009).
[9] P. Bonville *et al.*, Hyperfine Interact. **156/157**, 103 (2004); arXiv:cond-mat/0306470.
[10] S. T. Bramwell *et al.*, J. Phys. Condens. Matter **12**, 483 (2000); J. A. Hodges *et al.*, J. Phys. Condens. Matter **13**, 9301 (2001).
[11] H. W. J. Blöte, R. F. Wielinga, and W. J. Huiskamp, Physica (Amsterdam) **43**, 549 (1969).
[12] Y. Yasui *et al.*, J. Phys. Soc. Jpn. **72**, 3014 (2003).
[13] J. S. Gardner *et al.*, Phys. Rev. B **70**, 180404(R) (2004).
[14] J. A. Hodges *et al.*, Phys. Rev. Lett. **88**, 077204 (2002).
[15] K. A. Ross *et al.*, Phys. Rev. Lett. **103**, 227202 (2009).
[16] P. Santini *et al.*, Rev. Mod. Phys. **81**, 807 (2009).
[17] H. Cao *et al.*, Phys. Rev. Lett. **103**, 056402 (2009).
[18] H. B. Cao *et al.*, J. Phys. Condens. Matter **21**, 492202 (2009).
[19] B. Z. Malkin *et al.*, J. Phys. Condens. Matter **22**, 276003 (2010).
[20] J. D. Thompson *et al.*, J. Phys. Condens. Matter **23**, 164219 (2011).
[21] P. A. McClarty *et al.*, J. Phys. Conf. Ser. **145**, 012032 (2009).
[22] M. Elhajal *et al.*, Phys. Rev. B **71**, 094420 (2005).
[23] M. Enjalran and M. J. P. Gingras, Phys. Rev. B **70**, 174426 (2004).
[24] See supplemental material at http://link.aps.org/supplemental/10.1103/PhysRevLett.106.187202.
[25] J. Jensen and A. R. Mackintosh, *Rare Earth Magnetism* (Clarendon Press, Oxford, 1991).
[26] Y.-J. Kao *et al.*, Phys. Rev. B **68**, 172407 (2003).
[27] P. J. Brown in *International Tables for Crystallography*, edited by A. J. C. Wilson (Kluwer Academic Publishers, Dordrecht, 1992), Vol. C p. 393.
[28] T. Yavors'kii *et al.*, Phys. Rev. Lett. **101**, 037204 (2008).
[29] W. H. Press, S. A. Teukolsky, W. T. Vetterling, and B. P. Flannery *Numerical Recipes: The Art of Scientific Computing* (Cambridge University Press, Cambridge, England, 2007).
[30] S. W. Lovesey, *Theory of Neutron Scattering from Condensed Matter* (Clarendon Press, Oxford, 1984).